The catalytic mechanism of electron bifurcating electron transfer flavoproteins (ETFs) involves an intermediary complex with NAD^+

Gerrit J. Schut[1], Nishya Mohamed-Raseek[2], Monika Tokmina-Lukaszewska[3], David W. Mulder[4], Diep M. N. Nguyen[1], Gina L. Lipscomb[1], John P. Hoben[2], Angela Patterson[3], Carolyn E. Lubner[4], Paul W. King[4], John W. Peters[5], Brian Bothner[3], Anne-Frances Miller[2] and Michael W. W. Adams[1]*

[1]Department of Biochemistry and Molecular Biology, University of Georgia, Athens, GA 30602, USA. [2]Department of Chemistry, University of Kentucky, Lexington, Kentucky, USA. [3]Department of Chemistry and Biochemistry, Montana State University, Bozeman, Montana, USA. [4]Biosciences Center, National Renewable Energy Laboratory, Golden, Colorado, USA. [5]Institute of Biological Chemistry, Washington State University, Pullman, Washington, USA.

Running title: Mechanism for bifurcating electron transfer flavoproteins

*To whom correspondence should be addressed: Department of Biochemistry and Molecular Biology University of Georgia, Athens, GA 30602-7229 Tel: 706 542-2060. FAX: 706 542-0229 E-mail: adamsm@uga.edu

Keywords: Bifurcation, Bioenergetics, Flavin, Flavoprotein, Charge transfer, Radical; Semiquinone, Archaea, EtfABCX, anaerobic physiology

---

ABSTRACT (250 words)

Electron bifurcation plays a key role in anaerobic energy metabolism but it is a relatively new discovery and only limited mechanistic information is available on the diverse enzymes that employ it. Herein, we focused on the bifurcating electron transfer flavoprotein (ETF) from the hyperthermophilic archaeon *Pyrobaculum aerophilum*. The EtfABCX enzyme complex couples NADH oxidation to the endergonic reduction of ferredoxin and exergonic reduction of menaquinone. We developed a model for the enzyme structure by using non-denaturing MS, cross-linking and homology modeling in which EtfA, B, and C each contained FAD, whereas EtfX contained two [4Fe-4S] clusters. On the basis of analyses using transient absorption, EPR and optical titrations with NADH or inorganic reductants with and without NAD^+, we propose a catalytic cycle involving formation of an intermediary NAD^+-bound complex. A charge transfer signal revealed an intriguing interplay of flavin semiquinones and a protein conformational change that gated electron transfer between the low- and high-potential pathways. We found that despite a common bifurcating flavin site, the proposed EtfABCX catalytic cycle is distinct from that of the genetically-unrelated bifurcating NADH-dependent ferredoxin $NADP^+$ oxidoreductase (NfnI). The two enzymes particularly differed in the role of NAD^+, the resting and bifurcating-ready states of the enzymes, how electron flow is gated, and in the two two-electron cycles constituting the overall four-electron reaction. We conclude that *P. aerophilum* EtfABCX provides a model catalytic mechanism that builds on and extends previous studies of related bifurcating ETF's and can be applied to the large bifurcating ETF family.

Electron bifurcating enzymes couple exergonic and endergonic reactions, thus maximizing conservation of free energy available from exergonic reactions (1). In this way electrochemical energy can be captured for cellular metabolism lowering the demands on transmembrane gradients or substrate level phosphorylation. Thus, electron bifurcation provides a unifying explanation for many peculiar fermentative pathways found in anaerobic microorganisms, with important implications for understanding anaerobic microbial physiology in general (2-9).

So far the bifurcating enzymes that have been characterized fall into one of four phylogenetically-unrelated groups; electron transfer flavoproteins (EtfAB-containing), [FeFe]-hydrogenase/fomate dehydrogenases (HydABC-containing), heterodisulfide reductases (HdrA-containing) and transhydrogenases (NfnAB-containing) (8,10). These enzymes catalyze more than a dozen different reactions, most involving the oxidation or reduction of ferredoxin, and are found mainly in anaerobic organisms (reviewed in (3,8,11,12)). However, some of the EtfAB-containing complexes, such as that described below, can also be found in microaerophiles and aerobes.

Bifurcating ETFs are the best-studied bifurcating enzymes and they form a subset of the large and well-known family of ETFs, which are found in all domains of life (13-15). While the non-bifurcating ETFs contain one FAD and one AMP per AB heterodimer, the bifurcating EtfABs contain two FAD molecules, with the additional FAD replacing the AMP of the canonical ETF (13,16,17). The functions of bifurcating ETFs have been established in several strictly anaerobic micoorganisms. For example, the butyryl-CoA dehydrogenase (EtfAB-Bcd) complex from the butyrate-producing *Acidaminococcus fermentans* accomplishes the endergonic reduction of ferredoxin (Fd) with NADH by driving it with the exergonic reduction of crotonyl-CoA by NADH (16). Likewise, the strict anaerobe *Acetobacterium woodii* can utilize lactate as a carbon source using the bifurcating LDH-EtfAB complex to drive the endergonic oxidation of lactate to pyruvate with the energy provided by the exergonic electron transfer from reduced Fd to NAD^+ (18). *A. woodii* can also utilize caffeate as an electron acceptor in which EtfAB-containing caffeyl-CoA reductase complex (CarCDE) couples the exergonic reduction of caffeyl-CoA by NADH to the endergonic reduction of Fd by NADH (19). *Megasphaera elsdenii* similarly contains a lactate dehydrogenase and a Bcd that likely interact with the same EtfAB (20-22).

Bifurcating ETFs are also found in some microorganisms that are capable of fixing atmospheric nitrogen such as the aerobe *Azotobacter vinlandii* (13,23,24). In *A. vinlandii* an enzyme complex containing EtfAB and quinone reductase, termed FixABCX, is associated with nitrogen-fixing activity (13,24). The FixAB subunits are referred to as bifurcating Etf while the FixCX subunits are referred to as Etf-quinone oxidoreductase (13). FixABCX is thought to provide reduced Fd for nitrogen fixation through the quinone-dependent reduction of Fd with NADH (23,24). However genomic analyses reveal that FixABCX-like complexes are not restricted to diazotrophs indicating a general role extending beyond nitrogen fixation (13). We will refer to such complexes as EtfABCX to recognize their homology with FixABCX while also alluding to broader metabolic roles.

Herein we describe the mechanism for the first EtfABCX to be characterized from a non-nitrogen-fixing respiratory microorganism. Our exemplar was obtained from *Pyrobaculum aerophilum* (*Pae*), a denitrifying microaerophilic crenarchaeote that grows at 100°C. *Pae* oxidizes organic compounds using oxygen, nitrate, arsenate, selenate, iron and thiosulfate as terminal electron acceptors (25) but its genome lacks the genes for nitrogen fixation (26). The genes encoding *Pae* EtfABCX were expressed in the fermentative hyperthermophile, *Pyrococcus furiosus*, and both EtfABCX and the EtfAB subcomplex were purified. Like the Fix system (24), *Pae* EtfABCX is shown to oxidize NADH and bifurcate electrons to both high potential (quinone) and low potential (Fd) acceptors. For the *Pae* EtfABCX complex, we refer to each of the flavins in the enzyme in terms of the role that each has been proposed to play in ETF proteins in general (13,16,24,27). Thus, the FAD unique to bifurcating ETFs is denoted the 'bifurcating FAD' or BF-FAD and this is present in the A-subunit of *Pae* EtfABCX (**Figure 1**). The electron-transferring FAD or ET-FAD is the FAD that is shared with the structurally-homologous non-bifurcating ETFs that appear to specialize in electron transfer between partner proteins (13,14,28). By homology, the ET-FAD in *Pae* EtfABCX is located in the B subunit, while the FAD in the C subunit is referred to as the QR-FAD as it is likely the site of quinone reduction (**Figure 1**).

The primary goal of this work was to elucidate the overall catalytic cycle of *Pae* EtfABCX. Structural studies of related ETF

complexes have shown that large conformational changes occur during catalysis and a mechanism involving relatively large domain movement has been proposed (16,29,30). However more information is needed to understand how electron flow to the high and low potential acceptors is gated and controlled. It was also important to determine how the catalytic cycle of EtfABCX compared with that recently-established for the bifurcating enzyme, NADH-dependent ferredoxin NADP oxidoreductase I (NfnI) from *P. furiosus* (31). NfnI and EtfABCX have very similar cofactor compositions, even though they are completely unrelated phylogenetically, and both use NAD(P)H as the mid-potential donor to their BF-FADs and use Fd as the low potential carrier that is reduced or oxidized by a pair of [4Fe-4S] clusters (**Figure 1**). However, herein we have identified key catalytic intermediates of *Pae* EtfABCX, including a novel NAD$^+$-dependent charge-transfer complex, and describe a catalytic cycle that is very distinct from that established for NfnI. Moreover, the *Pae* EtfABCX catalytic cycle is consistent with previous structural observations and mechanisms of related EtfAB-containing complexes (8,9,13,24,27). We propose that the unifying principles proposed here can be applied to all bifurcating members of the large ETF family.

Results

Structure and catalytic activity of EtfAB and EtfABCX

The His-tagged form of *Pae* EtfABCX was produced in *P. furiosus*. Size exclusion chromatography of the purified enzyme resolved two peaks that corresponded (by mass spectrometric (MS) analysis) to EtfABCX, eluting near 450 kDa, and EtfAB, eluting near 50 kDa. The former is consistent with a tetrameric form of the EtfABCX complex (with a calculated mass of 125 kDa for the heterotetramer) while the latter peak corresponds to the EtfAB heterodimer (with a calculated mass of 66 kDa). Although EtfABCX is thought to interact with the cell membrane *in vivo* and to reduce quinone, the enzyme was purified from the cytoplasmic fraction of *P. furiosus*, is stable in solution and, in contrast to the FixABCX system (24), does not require detergent to maintain solubility. Analyses of *Pae* EtfAB by native MS gave the expected

mass with two FAD bound (measured: 69,562.45 Da; calculated: 69,566.17 Da, **Figure S1**). The A and B subunits were not separated by the collision energy during MS analysis, by reverse phase liquid chromatography under acidic conditions or by the presence of an organic solvent, implying great stability for the heterodimer. The EtfC subunit was also identified by MS with a mass consistent with a bound FAD cofactor (**Figure S2**). Based on MS analysis conducted under native and denaturing conditions, we conclude that as purified, both EtfAB and the EtfABCX holoenzyme have full flavin occupancy.

To predict the most probable 3D structure of individual subunits, the protein fold recognition tool Phyre2 was used (32). To determine the tertiary structure of the protein of interest, this relies on sequence alignment, secondary structure prediction and finally the match of predicted folds to homologous proteins with known protein structure. In the next step the energy minimized homology models of *Pae* Etf were overlaid on the structure of the recently published model of FixABCX from *A. vinelandii* (24). Once the quaternary structure was in place, cofactor-binding sites were modelled using individually refined models of *Pae* EtfAB, C or X, generated based on templates 1O97.pdb (EtfAB domain II), 4L2I.pdb (EtfAB, domains I and III), 2GMH.pdb (EtfC) and 2PVZ.pdb (EtfX) in Swiss Modeler, followed by manual adjustment of a few side chains and unstructured strands and then energy minimization.

To validate the structural model of the complete Pae EtfABCX complex, three complementary experimental approaches were employed: (1) non-covalent mass spectrometry to establish the mass of the entire complex in its native form, confirm the presence of cofactors, and determine cofactor and protein component stoichiometry; (2) chemical cross-linking and peptide-based mass spectrometry to ascertain protein-protein interaction networks and distance constraints; and (3) surface labeling coupled to mass spectrometry to map the solvent exposed surfaces. Iterative modeling was then used in which data from approaches 1-3 to test a model, identify inconsistencies, adapt the model and repeat (24,33-39). To preserve non-covalent interactions at protein interfaces the homobifuntional cross-linking reagent,

bis(sulfosuccinimidyl)suberate (BS3) was used. BS3 can probe a wide distribution of distances and bridge spatially close primary amine and hydroxyl containing amino acid residues (40). To probe solvent accessible surface of the intact complex and to obtain the most complementary results, two surface labeling reagents, glycine ethyl ester (GEE) and dansyl chloride (DnsCl) were used. GEE and DnsCl target carboxyl, primary amine, and hydroxyl groups, which collectively are the most prevalent groups on protein surfaces allowing for a detailed mapping of solvent exposed residues. The model shown in Figure 2 was in agreement with 37% of identified connections, including inter- and intra-subunit cross-links. Taking into account the distance a cross-linker can cover and the conformations a residue can adopt in solution, it is considered a good result if 30% of all generated cross-links within the complex are satisfied (33). Our best model was also in agreement with about 87% of the surface labels. The complete information on the generated cross-links and surface labels satisfying the *Pae* EtfABCX complex model can be found in **Table S1** and **Figure S3**, respectively.

The EtfABCX model shows that one of the [4Fe-4S] clusters in EtfX is within 10 Å of the BF-FAD, which should support rapid direct electron transfer. Although the BF- and ET-FAD are 16 Å apart and the distance between the isoalloxazine rings of the ET- and the QR-flavins is almost 30 Å, similar distances have been reported for the analogous flavins in the bifurcating EtfAB-Bcd and CarCDE complexes (29,30). Both of these complexes undergo a large conformational change as part of the catalytic cycle and such changes are also incorporated as part of the mechanism of *Pae* EtfABCX proposed herein.

Pae EtfABCX is thought to couple the reversible oxidation of NADH to the reduction of Fd and menaquinone (MQ), by analogy with FixABCX, according to Eqn. 1.

$$2NADH + 2Fd_{ox} + MQ \rightarrow$$
$$2NAD^+ + 2Fd_{red} + MQH_2 \qquad (1)$$
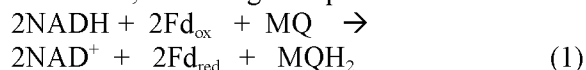
The primary Fd in *P. aerophilum* contains a single [4Fe-4S] cluster (41) and transfers a single electron (Eqn. 1), while MQ is thought to be the natural quinone component of the *Pae* respiratory system (42). The purified forms of both EtfAB

and EtfABCX catalyzed the oxidation of NADH and reduced the artificial electron carrier iodonitrotetrazolium (INT) with specific activities of 41.8 ± 6.5 and 15.8 ± 2.7 µmoles NADH oxidized/min/mg (at 80 °C), respectively. Although EtfC is proposed to reduce MQ *in vivo*, both EtfAB and EtfABCX also oxidized NADH and reduced the water soluble MQ analog, menadione. The specific activities were 8.8 ± 0.8 and 5.1 ± 1.2 µmoles NADH oxidized/min/mg (at 80 °C), respectively. The lack of specificity with respect to the quinone acceptor makes it difficult to directly measure the bifurcation activity of EtfABCX, which is further complicated by the fact that menadione and NADH have similar absorption spectra (24). Bifurcation activity of EtfABCX was therefore assessed by coupling the oxidation of reduced menadione and reduced Fd to the reduction of NAD$^+$, which was followed by the fluorescence of the NADH that was generated. The Fd used in this reaction was that of *P. furiosus*, which also contains a single [4Fe-4S] cluster (43). Importantly, reduction of NAD$^+$ by EtfABCX was dependent upon the presence of both reduced Fd and reduced menadione, and no bifurcation activity was detected using EtfAB (**Figure S4**). With the FixABCX from N$_2$-fixing *A. vinlandii*, a 25% increase in activity was observed when all substrates (NADH, quinone and Fd) were present relative to when only NADH and quinone were present (24), while in the case of *Pae* EtfABCX an approximately 2-fold increase was observed (**Figure S4**).

The reduction potentials of the flavins in EtfAB

The optical signatures of the two flavins of EtfAB were monitored over the course of stepwise reduction with sodium dithionite or Ti-citrate in the absence of mediators (**Figure S5A and S6**). The initial increase in absorbance at 374 nm, where the anionic semiquinone (ASQ) of flavin absorbs maximally, was accompanied by a decrease at 454 nm (absorption maximum of oxidized flavin) indicating that an FAD undergoes a 1 e$^-$ reduction to ASQ (**Figure S5, phase 1**). We assigned this to the ET-FAD as it is expected to be more readily reduced than the BF-FAD (17,27). Further addition of reductant resulted in only a slight intensity loss at 374 nm suggesting little change in the amount of ASQ (**Figure S5, phase 2, staggered or nested

4

mechanisms). As discussed further below, to account for these observations we propose that a radical is present on either the ET-FAD or the BF-FAD leading to the observed optical signal. This ASQ signal also persisted upon addition of excess Ti-citrate (this was also true with excess dithionite, though less clear: see **Figures S5A and S6**).

Titrations in the presence of redox mediators showed that one flavin undergoes reduction from OX to ASQ to HQ before the other is reduced from OX to HQ (**Figure S5C**, sequential). Thus, in **Figure S7A**, the initial negative difference absorbance near 374 nm clearly indicates that ASQ is formed while the positive intensity at 454 nm represents the OX signature lost in the course of this reaction (OX at the beginning exceeds OX at the end, **Figure S5A**). Conversion of the ET-FAD from OX to ASQ occurred with an E_m of 33 ± 6 mV (**Figure 3**). The slope of the line near 0.5 confirms that the reaction in question is a 1 e⁻ reaction and therefore rules out reduction to HQ. Difference spectra associated with phase 2 of the reductive titration (**Figure S5B**) indicate that it corresponds to net reduction of an ASQ to HQ (**Figure S7B**). These data clearly show net loss of the ASQ features. The slope of the Nernst log/log plot in **Figure 3** confirms this event as a 1 e⁻ reaction. The intercept of the Nernst log/log plot yields an E_m value for ET-FAD (ASQ/HQ) of -94 mV ± 7 mV. Titration of the lower potential FAD (**Figure S7C**, phase 3) reveals no significant contribution from ASQ and the slope of 1 of the Nernst log/log plot confirms that this phase corresponds to a 2 e⁻ reduction (**Figure 3A**). An E_m value for BF-FAD (OX/HQ) of -285 mV ± 5 mV was determined, which is close to the value of -279 mV reported for the bifurcating EtfAB from *M. elsdenii* (21). Thus, we conclude that the higher potential FAD, ET-FAD, is reduced via two sequential 1 e⁻ events to HQ but that the lower potential FAD, BF-FAD, undergoes reduction directly to the HQ state in a 2 e⁻ event under equilibrium conditions (**Figure 3B**). The values measured for *Pae* EtfAB of $E_{m(OX/ASQ)}$ = +33 mV and $E_{m(ASQ/HQ)}$ = -94 mV fall well within values reported for other EtfABs (21,27) and the high $E_{m(OX/ASQ)}$ of +33 mV for *Pae* EtfAB indicates that the resting state of the EtfAB dimer possesses ET-FAD in its ASQ state.

Transient absorption spectroscopy of EtfAB and EtfABCX

The SQ state of the BF-FAD was not observed in steady state titrations so transient absorption spectroscopy (TAS) was used to probe for short-lived flavin species. Formation of an ASQ with loss of absorption from the oxidized flavin was observed for both EtfAB and EtfABCX (**Figure S8**). In each, the ASQ kinetic trace was best fit with two components corresponding to lifetimes of 60 and 1080 ps, suggesting that they arise from distinct flavins that are present in both EtfAB and EtfABCX. We therefore assigned the 60 and 1080 ps SQ components to the BF- and ET-FAD, respectively, based on the titration results that show the BF-FAD generates a more thermodynamically unstable ASQ than ET-FAD. In addition to the ASQ signal, we also observed the presence of a signal at ~570 nm suggesting that there is emission from FAD OX, the origin of which is unknown (Figure S8A). The formation of flavin SQ states was further studied by visible and EPR spectroscopy, as discussed below.

Reductive titrations of EtfAB

The spectral features around 374 nm of as purified EtfAB were assigned to an ASQ and this was converted to the fully oxidized form by exposure to air (**Figures 4A** and **S6**). Stepwise reduction of air-oxidized EtfAB with NADH regenerated the ASQ seen in the as-purified complex (prior to air oxidation), as indicated by spectral features at 374 nm with a shoulder at 398 nm. These reached a maximum with the addition of about half an equivalent of NADH (**Figures 4A** and **S9**). To explain how a two-electron hydride transfer from NADH generates a singly-reduced ASQ state on the ET-FAD, we propose intermolecular electron transfer between two EtfAB molecules, as was suggested for the NADH-induced ASQ state of the related EtfAB-Bcd complex of *A. fermentans* (16,29). These data with *Pae* EtfAB therefore confirm the conclusion from the equilibrium titrations that the ET-FAD rests in the ASQ state when the complex is 'ready' for bifurcation. EtfAB appeared fully reduced upon further addition of NADH to more than two equivalents, as shown by the lack of absorption at 454 nm. In addition, a strong charge

transfer (CT) band feature is seen from 550 to 1000 nm (**Figures 4A** and **S9**). The reduction of *A. fermentans* EtfAB with NADH showed a similar absorption spectrum although the CT band was not as obvious (16). The CT band has to arise from the interaction of NAD^+ with the BF-FAD because the ET-FAD does not interact with NAD(H) (13). Considering that NADH adds two electrons to the EtfAB core there must be a flavin radical present (with three electrons distributed between two FAD cofactors), however, this is not obvious from the UV-vis spectrum.

EPR spectroscopy was used to directly probe for the presence and nature of radical species (44,45). *Pae* EtfAB as purified anaerobically in the absence of reductants displayed a weak radical centered at $g = 2.006$ (0.1 spin mol^{-1}) and this increased slightly (to 0.2 spin mol^{-1}) upon addition of NADH (**Figure 5**). In contrast, reduction of EtfAB with excess sodium dithionite produced an intense anisotropic radical signal centered at $g = 2.007$ representing ~1.0 spin mol^{-1}. The narrow line-width (14 G) is indicative of an ASQ radical (46), in agreement with the absorption data (see below) indicating that an ASQ radical is the source of this signal, however is not clear if the radical resides on the BF- or ET-FAD. Addition of NAD^+ to the dithionite-reduced sample decreased the EPR absorption by 50%, and broadened the line-width of the radical signal (from 14 to 20 G). Although change in line-width is suggestive of a neutral semiquinone (NSQ) flavin radical (45), this broadening of the radical signal more likely reflects interactions of the BF-FAD with NAD^+ affecting the optical and paramagnetic signal of the ASQ radical.

Similarly, treatment of *Pae* EtfAB with the chemical reductant Ti-citrate (**Figure S6**) generated an ASQ state that persisted even in the presence of excess reductant (**Figure 4C**). We propose that this corresponds to the 3 e⁻ reduced state of EtfAB. However, upon addition of NAD^+ to Ti-reduced EtfAB, the optical ASQ signature is lost and a CT complex is generated (**Figures 4C** and **S10**). It should be noted that this CT signature is slightly different (less absorbance in the 680 nm region) from that observed after treatment of EtfAB with excess NADH, where NAD^+ is generated *in situ* (compare **Figures S9**

and **S10**). These data confirm that NAD^+ binding to the BF-FAD site changes the electronic state of the EtfAB core whereby the usual absorption spectrum of the ASQ is not observed even though a radical can be seen by EPR analysis (**Figure 5**). Thus, it appears that a 3 e⁻ reduced state of EtfAB accumulates upon reduction with NADH and by chemical reductant, based on both optical and EPR spectroscopy.

Reductive titrations of EtfABCX

The response of EtfABCX to chemical reductants and to NAD(H) was similar to that of EtfAB (**Figures 4, S11** and **S12**) but more complex due to the additional flavin (QR-FAD) in EtfC and the two [4Fe-4S] clusters in EtfX. Titration of EtfABCX with NADH forms an intermediate ASQ that disappears and is replaced by absorption from an NSQ near 620 nm, mixed with the broad absorption of the CT complex which we assigned to the interaction of NAD^+ with the EtfAB core (**Figure S12**). The additional flavin radical (the NSQ) we assigned to the QR-FAD in EtfC. A strong semiquinone radical signal (0.5 spins mol^{-1}) at $g = 2$ was observed upon reduction of EtfABCX with excess NADH, in addition to several overlapping broad signals spanning the $g = 2.08 - 1.80$ region indicative of reduced iron-sulfur clusters (**Figure 5**). The semiquinone EPR signal centered at $g = 2.006$ was resolved at 77 K. The line-width (20 G) is most consistent with it originating from an NSQ radical (45) (**Figure 5C**), possibly from the QR-FAD in EtfC (**Figure 1**). The broad EPR signals were most intense near 10 K and disappeared above 30 K (**Figure 5G**), consistent with the relaxation properties of reduced $[4Fe-4S]^{1+}$ clusters. The reduction potentials of the two [4Fe-4S] clusters in *P. furiosus* Nfn (see **Figure S13**) were estimated at -513 mV and -718 mV by direct electrochemistry (31) but unfortunately *Pae* EtfABCX was not responsive to this approach.

The reduction by NADH of the lower potential [4Fe-4S] clusters of EtfX is further evidence of the bifurcating activity of *Pae* EtfABCX, as is formation of the QR-FAD of EtfC to generate a NSQ seen by visible absorption. In addition, NAD^+ also interacts with chemically-reduced *Pae* EtfABCX yielding CT bands but, as with EtfAB, the spectrum is slightly

different (lacking some of the 680 nm features) from that induced by NADH treatment alone, indicating that the CT bands are an inherent property of the interaction of NAD$^+$ with the EtfAB core.

Discussion

The data presented herein show that the *Pae* EtfAB core possesses several crucial prerequisites for bifurcating activity: 1) a bifurcating flavin that accepts electron pairs from NADH, 2) a high potential electron transfer pathway consisting of a high potential flavin (E_m = -94 mV for the ASQ/HQ couple of ET-FAD) linking the bifurcating flavin to the quinone pool via QR-FAD, and 3) a low potential pathway by which the BF-FAD reduces Fd (via the two 4Fe-clusters in EtfX). Our measured E_m (-285 mV) for the OX/HQ couple of BF-FAD is more positive than that of NADH ($E^{0'}$ -320 mV) indicating favorable electron transfer but with minimal dissipation of energy. However, the BF-FAD does not display a stable SQ state in our mediated equilibrium titrations, which suggests that it exhibits crossed potentials where its E_m ASQ/HQ is more positive than its E_m OX/ASQ, although their average must correspond to the measured E_m OX/HQ of -285 mV (ASQ is proposed based on its observation by TAS). Thus, we can calculate a lower limit for the E_m of the BF-FAD ASQ/HQ couple. Assuming that the ASQ/HQ couple of the ET-FAD is operative in turnover (27,30), electron transfer to ASQ-ET-FAD at -94 mV is exergonic by 191 mV. It follows that electron transfer to Fd can be endergonic at a similar level, placing a lower boundary of -476 mV on the E_m of the BF-FAD OX/ASQ, which is presumably sufficient to reduce Fd (3,47). For the respiratory bifurcating bc$_1$ complex, a stability constant for the low potential SQ state of the bifurcating quinone was estimated at approximately 10^{-15}, from which a potential span of ~900 mV between the first high potential electron versus the second low potential electron was derived (48). This concept has been adapted to calculate the potentials of other bifurcating centers, including several EtfAB-containing complexes (reviewed in (8)). Although the quinone value does not apply to a flavin system, which has very different chemistry, it puts our value in perspective. When it is applied to *Pae* EtfABCX, we calculate a

ASQ/HQ couple of +165 mV (-285 +(900 mV/2) and an OX/ASQ couple of -735 mV (-285 –(900 mV/2). Hence, based on these two approaches, we estimate the E_m of ASQ/HQ to be between -94 and +165 mV while that of OX/ASQ to be between -735 and -476 mV, with an average corresponding to the measure value of -285 mV. These values are well within the range proposed previously for other Etf-type complexes and are consistent with the thermodynamically favorable reduction of Fd with an E_m of approximately -500 mV (8,30,48).

As shown in **Figure 6**, we propose that, based on the equilibrium titration data, the 1 e$^-$ reduced state of EtfAB within the EtfABCX complex is the resting form of the enzyme. This accepts a hydride from NADH to generate the HQ-BF-FAD in close proximity to ASQ-ET-FAD, in which the NAD$^+$ stays bound and forms a NAD$^+$•BF-FAD$_{HQ}$ CT complex. The BF- and ET-FAD could share an electron switching between HQ-BF-FAD/ASQ-ET-FAD and ASQ-BF-FAD/HQ-ET-FAD and the stable CT complex is formed by the strong interaction of NAD$^+$ with BF-FAD, as shown in **Figure 6**. In this state the EtfAB subcomplex is 'hot' and can transfer the low potential electron from the BF-FAD to Fd through the proximal and distal iron sulfur clusters in EtfX, leaving the EtfAB subcomplex as OX-BF-FAD/HQ-ET-FAD. The distance between the ET-FAD and the QR-FAD is too far for efficient electron transfer (**Figure 2** and (16,21,29,30,49)) but it has been proposed that ETF-type complexes undergo a large conformational change as part of the catalytic cycle (16,21,29,30). We suggest that this is triggered by oxidation of the ASQ-BF-FAD and brings the ET-FAD close enough to the QR-FAD for electron transfer into the high potential active site (30). The high potential electron on HQ-ET-FAD cannot reduce the highly crossed BF-FAD and so it can only be transferred to EtfC, thereby returning the EtfAB core to its bifurcation-ready 1 e$^-$ reduced state (**Figure 6**). It is not clear when NAD$^+$ leaves the EtfAB core, but we assume it is after or in conjunction with transfer of the low potential electron from the BF-FAD.

Once the 1 e$^-$ reduced EtfAB core of EtfABCX is generated by loss of the high potential electron, the enzyme then undergoes a second round of reduction by NADH. Note that

7

only the first round of NADH oxidation is shown in **Figure 6**. Hence, to complete the overall 4 e⁻ reaction (Eqn. 1), a second NADH binds, a second molecule of Fd is reduced via EtfX, and a second electron is transferred to NSQ-QR-FAD, which in its fully reduced HQ form reduces one molecule of MQ. Thus, the two rounds of bifurcation that constitute the catalytic cycle of EtfABCX (Eqn. 1) are in essence the same in terms of the BF- and ET-FAD, where the second NADH interacts with the same bifurcation-ready 1 e⁻ reduced form of the EtfAB sub-complex as the first NADH.

It is important to point out that our proposed mechanism (**Figure 6**) eliminates the possibility of the second electron from BF-FAD passing to the ET-FAD, despite the favorable thermodynamics, because the ET-FAD is fully reduced to its HQ state upon accepting the first electron derived from NADH and therefore is unable to accept a second electron (30). Thus, the strongly-reducing electron of the ASQ-BF-FAD would be constrained to use the low potential branch formed by the [4Fe-4S] clusters in EtfX. In contrast, our *in vitro* reductions of fully oxidized EtfAB enable NADH to provide two electrons and reduce the ET-FAD from the OX to the HQ state, whereupon electron transfer between HQ-ET-FAD-EtfAB and OX-ET-FAD-EtfAB generates two ASQ-ET-FAD-EtfAB thereby explaining the formation of the ASQ state during NADH titrations (**Figures 4A and S9**). This was also proposed for the related EtfAB-Bcd complex (16). This ASQ state is also formed in the *Pae* EtfABCX complex when all partners are present (**Figure 4B and S12**).

Reduction of *Pae* EtfAB and EtfABCX by NADH generates a striking CT band spanning 600 to 1000 nm (**Figures 4A** and **4B**) with little absorbance remaining at 454 nm. Chemical reduction of EtfAB and EtfABCX both generate a flavin ASQ that does not undergo further reduction with excess reductant (**Figure S6 and S11**) and upon NAD⁺ binding the optical ASQ signal disappears and a CT signal appears instead (**Figure 4C and S11**). Previous reports on related ETF systems from mesophilic organisms either do not collect data for the full 600 to 1000 nm region or report much weaker absorption (16,21). We propose that the much stronger signal seen from the *Pae* proteins is a consequence of the

hyperthermophilic organism that we have used as the gene donor to produce EtfABCX. The optical spectra were collected at room temperature, which is 80°C lower than the optimum growth temperature of *P. aerophilum* (25). In contrast, the related Etf systems caffeyl-CoA reductase (CarCDE), butyryl-CoA dehydrogenase-Etf and FixABCX derive from mesophilic microorganisms (4,19,24). The enhanced stability of hyperthermophilic enzyme might intensify the effect of NAD(H) binding leading to more distinct spectral features for the CT complexes.

With *Pae* EtfABCX we experimentally distinguished two different CT optical signatures. Both have a broad CT feature with a maximum around 780 nm but if NADH is used as the reductant a second feature is seen near 680 nm (**Figure 4A, 4B, S9** and **S12**). From our data the CT complex is formed by NAD⁺ binding to the BF-FAD and a flavin radical is present. We propose that both BF-FAD and ET-FAD are electronically coupled and influence the nature of the NAD⁺-bound complex. It was previously suggested for a related EtfAB complex that a tyrosine residue situated between the BF-FAD and ET-FAD mediates an electronic coupling between the two flavin cofactors (27). In *Pae* EtfAB a tryptophan residue occupies this position and would also be competent to mediate such a coupling. While a charge transfer between NADH and the OX-BF-FAD could also be possible (50,51), this is inconsistent with both the radical EPR signal and the absence of an optical signature expected from the ET-FAD ASQ. The exact nature of the NAD⁺-bound complexes in *Pae* EtfABCX is therefore unclear at present.

The reaction mechanism of *Pae* EtfABCX involves a bifurcating flavin with crossed potentials where removing one electron from the HQ state generates a high energy intermediate (ASQ) with a potential lower than that of the donor electron pair (from NADH) that is capable of ultimately reducing Fd (1,31), although it should be noted that crossed potentials may not be an absolute requirement for bifurcating activity (52). It is generally accepted that this ASQ derived from a highly crossed BF-FAD is 'unstable' (53). In our new NAD⁺-dependent mechanism, we propose that the formation of a NAD⁺ BF-FAD complex might

protect this high energy low potential site from potentially harmful chemical reactions, especially when the EtfAB core is not complexed with its partners (**Figure 6**). For example, it was previously shown that molecular oxygen can be reduced by the analogous EtfAB-Bcd complex and this leads to formation of superoxide with potentially disastrous consequences for the cell (22). Based on our reaction scheme (**Figure 6**), we propose that the addition of NADH to the EtfAB-Bcd complex also forms a NAD$^+$ BF-FAD complex and that, in the absence of the high potential substrate (crotonyl-CoA), this minimizes reaction of the BF-FAD with oxygen. Protection of a flavin site from oxygen through formation of a NAD$^+$ complex to prevent the formation of damaging superoxide has been shown before with enzymes such as toluene dioxygenase and NADH quinone oxidoreductase (54,55). The formation of a NAD$^+$ charge transfer complex might therefore be an integral feature of EtfAB complexes and play an important role not only in its mechanism but also in protecting the cell from reactive oxygen species, a particularly important feature in (micro)aerophilic microorganisms, such as *P. aerophilum* (8,29,30,48). Unexpectedly, we did not observe the complete 4 e$^-$ reduced form of EtfAB (or the EtfABCX equivalent) with either the physiological electron donor NADH or with an artificial reductant. This interesting characteristic of the EtfAB core is presumably related to the formation of the NAD$^+$ BF-FAD complex although the reason for this and the detailed nature of the different electronic states will be a topic of future studies.

The only other type of bifurcating enzyme that has been studied in detail mechanistically is the phylogenetically-unrelated NfnI of *P. furiosus* (31). At first glance this catalyzes a similar reaction to that of *Pae* EtfABCX, except that the high potential acceptor is NAD rather than quinone (**Figure 1**). However, other than a common site (BF-FAD) to bifurcate the two electrons from the hydride transfer from NAD(P)H, the proposed catalytic cycle of *Pae* EtfABCX (**Figure 6**) is very different from that of NfnI (**Figure S13**). In both enzymes, reduction of BF-FAD by NAD(P)H provides electrons for the high and low potential pathways but the stable nicotinamide-dependent CT complex observed

with EtfABCX is not evident with NfnI. In further contrast, the 1 e$^-$ reduced form of EtfABCX with the ASQ state of the ET-FAD is the proposed physiological resting form, which is ready to accept a hydride from NADH to form 3 e$^-$ reduced intermediates. However, the resting state of NfnI is fully oxidized and its reduction by NADPH generates a stable 2 e$^-$ reduced state (**Figure S13**). Moreover, in Nfn, the subsequent oxidation of ASQ-BF-FAD by reduction of ET-FAD is gated by an intervening [2Fe-2S] cluster, which mediates electron flow via the ET-FAD to the high potential acceptor (in this case, NAD$^+$) in the absence of any significant conformational change (56). In further contrast, electron flow to the high potential pathway in EtfABCX is gated by a flavin 1 e$^-$ acceptor and a rather dramatic conformational change that enables oxidation of ET-FAD (31).

The results presented herein therefore show that, in spite of a common bifurcating flavin, *Pae* EtfABCX and *P. furiosus* NfnI differ by formation of a stable nicotinamide-dependent CT complex in the former and not the latter, in the nature of the resting and bifurcating-ready states of the enzymes, in how electron flow down the exergonic path is gated, and in the two 2 e$^-$ catalytic cycles that constitute the overall 4 e$^-$ bifurcation reaction. They also differ in the overall energetics of their reactions. While both reduce Fd (E_m ~-500 mV), the driving force for EtfABCX ($\Delta E = 250$ mV) is derived from NADH oxidation ($E^{0'} = -320$ mV) coupled to MQ reduction ($E^{0'} = -70$ mV). This provides more than twice the driving force for bifurcation than in NfnI ($\Delta E = 100$ mV), which couples the oxidation of NADPH (E_m ~-380 mV, under physiological conditions) to the reduction of NAD$^+$ (E_m ~-280 mV). It is not clear if the overall energetics are related to any differences in the overall catalytic cycles for the two enzymes. This emphasizes that there might not be a general flavin-based bifurcating mechanism, rather each type of enzyme harbors a unique reaction scheme (3,8,11,12). Nevertheless, the reaction scheme shown in **Figure 6** is proposed as a framework to guide future work in elucidating more mechanistic details of the bifurcating reaction of *Pae* EtfABCX and of bifurcating ETFs in general.

9

Experimental procedures

Expression and purification of P. aerophilum EtfABCX

The plasmid encoding *Pae* EtfABCX was constructed with the following fragments via Gibson Assembly (NEB): a 8.8 kb backbone BAC vector containing the *pyr*F genetic marker, the flanking homologous recombination region targeting the interspace between convergent genes PF1232 and PF1233, the *slp* promoter region (PF1399) and the 5.04 kb EtfBAXC genes PAE0721-0723, with a 9xHistidine-Alanine tag at the N-terminal of the EtfA subunit (PAE0725). The order of genes in this cluster was rearranged to EtfABCX (PAE0722, PAE0721, PAE0725 and PAE0723) with a *P. furious* ribosomal binding site inserted in front of each Etf subunit. This plasmid, termed pGL098, was sequence verified and linearized before transformation of *P. furiosus* COM1 strain as previously described (57). Positive transformants were cultured and purified twice on liquid and solid defined cellobiose medium. The genomic DNA was isolated using ZymoBeadTM Genomic DNA Kit (Zymo Research) and PCR was used for isolates screening, using a primer pair that target outside the homologous flanking region mentioned above. The strain containing the EtfABCX overexpression construct was designated as MW393. All primers used in plasmid and strain construction are listed in **Table S2**.

Large scale fermentation of recombinant *P. furiosus* was performed as previously described (58). Frozen cells (~100 g wet weight) were lysed in 50 mM phosphate buffer, pH 7.5, with 1 mM DTT under strict anaerobic conditions. Cell debris and membranes were removed by centrifugation at 100,000 g. The supernatant was loaded on a 5 ml Histrap column (GE) using the recommended phosphate buffer with the addition of 1 mM DTT. The green colored EtfABCX started eluting when ~50 mM imidazole was applied. Based on the chromatogram, the green/yellow fractions were pooled and concentrated to ~5-10 ml using ultrafiltration under anaerobic conditions. The concentrated sample was applied to a Superdex S200 column (60/600; GE) and eluted with 25 mM TrisHCl, pH 8, containing 300 mM NaCl (but lacking DTT). Fractions corresponding to EtfAB and EtfABCX were selected on the basis of flavin content and gel electrophoresis (Miniprotean TGX stainfree gels, BioRad).

Enzyme assays

NADH-linked activities of EtfAB and ABCX were measured anaerobically at 80°C in 3-ml glass cuvettes sealed with rubber stoppers containing 50 mM HEPES, pH 7.5, 100 mM NaCl, 1 mM NADH, and 200 μM iodonitrotetrazolium chloride (INT). The formation of the red formazan was followed at 500 nm (ε = 19.3 mM^{-1} cm^{-1}) in a 100 Cary UV-Vis spectrophotometer with a peltier-based temperature controller (Agilent). When menadione (100 μM) was used as electron acceptor, the activity was followed by the oxidation of NADH (200 μM, ε = 6.2 mM^{-1} cm^{-1} at 340 nm). Bifurcating assays were performed anaerobically in quartz 4 ml fluorescence cuvettes sealed with silicon stoppers using a RF-5301-PC fluorimeter (Shimadzu). *P. furiosus* Fd (50 μM) and menadione (100 μM) were reduced with 400 μM Ti-citrate (reduction of Fd was monitored by its UVvis spectrum). NAD$^+$ (1 mM) was added as electron acceptor and the formation of NADH was followed by fluorescence, ex 340 nm/em 460 nm.

Redox titrations

Titrations were performed at 25°C in an upcycled Agilent HP 8453 operating under OlisWorks (Olis) using 600 μl masked quartz cuvettes (Starna) anaerobically sealed with silicon stoppers. Reductant was anaerobically added in small quantities with a 10 μl gastight syringe (Hamilton) to samples prepared in 50 mM MOPS pH 7.5 with 200 mM NaCl. UVvis spectra, 200-1000 nm, were recorded after each addition. All solutions were prepared under strict anaerobic conditions and stock solutions of titanium citrate were prepared as previously described (59).

To determine reduction midpoint potentials at pH 7.0 ($E^{0'}$), protein samples were prepared in 25 mM bis-Tris-propane, pH 7.0, containing 200 mM NaCl. $E^{0'}$ values were measured using the xanthine/xanthine oxidase system (27,60,61). Attainment of equilibrium was confirmed by comparing $E^{0'}$ values obtained in slower and faster titrations, 40 min was typical (62) and all titrations were performed in duplicate

or more. The dyes used were thionin acetate (n_{Dye}=2, $E^{0'}_{Dye}$ = +56mV, λ_{max} = 598 nm), nile blue chloride (n_{Dye} = 2, $E^{0'}_{Dye}$ = -116 mV, λ_{max} =636 nm), safranin-O (n_{Dye} =2, $E^{0'}_{Dye}$ = -289 mV, λ_{max} =520 nm and the dye isosbestic at 412 nm was used for monitoring the flavin). Data were analyzed using Eqn. 2 derived by equating the Nernst equation for the dye to that of the enzyme, at equilibrium with the dye, for the example of the OX/ASQ couple. At each point in the titrations

$$log_{10}\frac{[Ox_{FAD}]}{[Red_{FAD}]} = \frac{n_{FAD}}{n_{Dye}}log_{10}\frac{[OX_{Dye}]}{[Red_{Dye}]} + $$
$$\frac{n_{FAD}\,F}{RT\,ln10}\left(E^0_{Dye} - E^0_{FAD/FAD^{\bullet -}}\right) \quad (2)$$

the concentrations of oxidized and reduced dye and reacting flavin were determined from the absorbance values of each at the appropriate wavelength. To focus on only the one flavin undergoing reduction in each phase of reduction, difference spectra were used. In these, the final spectrum of each phase was subtracted from each other spectrum in the phase and the three phases were identified by noting the different changes in A_{374} characterizing initial reduction of OX to ASQ, ASQ to HQ and OX to HQ (**Figure S6**). Thus we calculated the concentration of FAD or dye remaining in the oxidized state of the reaction under consideration ([Ox_{FAD}] or [Ox_{dye}]) and from these and the total concentrations we obtained the concentrations of the corresponding reduced states ([Red_{FAD}] or [Red_{dye}]). Plots of $log_{10}\frac{[Ox_{FAD}]}{[Red_{FAD}^{\bullet -}]}$ vs $log_{10}\frac{[OX_{Dye}]}{[Red_{Dye}]}$ then yielded n_{FAD}, the number of electrons taken up by the FAD revealing the nature of each reaction, from the magnitude of the slope, m = n_{FAD}/n_{dye}. The intercept with the vertical axis at log([Ox_{dye}]/[Red_{dye}])=0, b, then yielded the flavin $E^{0'}$ of the reaction from b = $n_{FAD}(E^{0'}_{Dye}$-$E^{0'}_{FAD})$/25.7 mV, where 25.7 mV replaces the physical constants and temperature RT/F (T = 25 °C) and all $E^{0'}$ values are quoted vs. the normal hydrogen electrode.

EPR spectroscopy

Samples of *Pae* EtfAB and EtfABCX were prepared for analysis by EPR spectroscopy under strictly anaerobic conditions in a N_2 atmosphere glove-box (MBraun). Both EtfAB (150 μM) and EtfABCX (120 μM) were prepared in 25 mM Tris buffer containing 300 mM NaCl and 5% (v/v) glycerol. EtfAB was treated with either NADH (1 mM), Na-dithionite (10 mM), or sequential treatments of Na-dithionite (10 mM) and NAD$^+$ (10 mM). For the latter, NAD$^+$ was added to a thawed sample that had been initially treated and frozen with Na-dithionite. All samples were prepared in sealed tubes and slowly frozen in liquid N_2. EPR spectra were recorded with a Bruker E-500 spectrometer (X-band, 9.38 GHz) equipped with a SHQ resonator, an in-cavity cryogen free VT system (ColdEdge Technologies) and MercuryiTC temperature controller (Oxford). EPR parameters for measuring radical signals were as follows: modulation frequency, 100 kHz; modulation amplitude, 2 G; microwave power, 1 mW; temperature, 77 K. EPR parameters for measuring [Fe-S] signals were as follows: modulation frequency, 100 kHz; modulation amplitude, 10 G; microwave power, 1 mW; temperature, 10 K. Spin quantification of radical signals were carried out by comparison of signal intensities to standards using HO-TEMPO (4-hydroxy-2,2,6,6-tetramethylpiperidine 1-oxy, 5 - 100 μM concentration) and double integration of the spectra using the OriginPro software package.

Transient absorption spectroscopy (TAS)

The ultrafast (100 fs to 5.1 ns) TAS spectrometer employed here was operated as previously described (31). The pump wavelength was 400 nm for sample excitation, and the experiment was conducted at room temperature. For all measurements, the sample was prepared in an Mbraun glove-box (N_2 atmosphere), sealed in a 2 mm quartz cuvette and constantly stirred to prevent photodegradation. The concentrations of *Pae* EtfAB and EtfABCX were approximately 150 μM and 100 μM, respectively. The data collection (350 pump shots per time point) was carried out four consecutive times and then averaged. The experiment was repeated two times. Data were corrected for spectral chirp using SurfaceXplorer (Ultrafast Systems). Fitting was performed in Igor Pro using a single or double exponential fit functions.

Mass spectrometric analysis

Protein identification (63), intact protein analysis (64) and protein-protein interactions analysis (24,65) were performed as previously described. The *Pae* EtfABCX complex (7.9 μM) was surface labeled with 0.3 mM DnsCl (Acros) in a 100 mM sodium phosphate buffer, pH 8.0 at 25°C. The reaction was quenched after 5, 15 and 30 mins with 2 μl of 100 mM ammonium acetate, pH 8.0. Samples were digested with trypsin followed by LCMS/MS analysis (63). Native-MS experiments were conducted on a SYNAPT G2-*Si* instrument (Waters) (66). Samples were exchanged to 500 mM ammonium acetate, pH 7.0 (Sigma) and infused from in-house prepared gold-coated borosilicate glass capillaries at a protein concentration of 1.5 μM and a flow rate of 90 nl min^{-1}. Data analysis was performed in MassLynx software version 4.1 (Waters). The EtfABCX model was produced using Swiss Modeler (67), followed by manual adjustment of a few side chains and unstructured strands and then energy minimization in Chimera (68). These were tested on the basis of the fit of the cofactors from the template structures within the modeled *Pae* components.

Conflict of interest: The authors declare that they have no conflicts of interest with the contents of this article.

References

1. Peters, J. W., Miller, A. F., Jones, A. K., King, P. W., and Adams, M. W. (2016) Electron bifurcation. *Curr Opin Chem Biol* **31** 146-152
2. Brandt, U. (1996) Bifurcated ubihydroquinone oxidation in the cytochrome bc1 complex by proton-gated charge transfer. *FEBS Lett* **387** 1-6
3. Buckel, W., and Thauer, R. K. (2013) Energy conservation via electron bifurcating ferredoxin reduction and proton/Na$^+$ translocating ferredoxin oxidation. *Biochim. Biophys. Acta.* **1827** 94-113
4. Li, F., Hinderberger, J., Seedorf, H., Zhang, J., Buckel, W., and Thauer, R. K. (2008) Coupled ferredoxin and crotonyl coenzyme A (CoA) reduction with NADH catalyzed by the butyryl-CoA dehydrogenase/Etf complex from *Clostridium kluyveri*   *Bacteriol* **190** 843-850
5. Metcalf, W. W. (2016) Classic spotlight: electron bifurcation, a unifying concept for energy conservation in anaerobes.   *Bacteriol* **198** 1358
6. Mitchell, P. (1976) Possible molecular mechanisms of the protonmotive function of cytochrome systems.   *Theor Biol* **62** 327-367
7. Schut, G. J., and Adams, M. W. (2009) The iron-hydrogenase of *Thermotoga maritima* utilizes ferredoxin and NADH synergistically: a new perspective on anaerobic hydrogen production. *J Bacteriol* **191** 4451-4457
8. Buckel, W., and Thauer, R. K. (2018) Flavin-based electron bifurcation, a new mechanism of biological energy coupling. *Chem Rev* **118** 3862-3886
9. Herrmann, G., Jayamani, E., Mai, G., and Buckel, W. (2008) Energy conservation via electron-transferring flavoprotein in anaerobic bacteria.   *Bacteriol* **190** 784-791
10. Buckel, W., and Thauer, R. K. (2018) Flavin-based electron bifurcation, ferredoxin, flavodoxin, and anaerobic respiration with protons (Ech) or NAD$^+$ (Rnf) as electron acceptors: A historical review. *Front Microbiol* **9** 401
11. Peters, J. W., Beratan, D. N., Schut, G. J., and Adams, M. W. W. (2018) On the nature of organic and inorganic centers that bifurcate electrons, coupling exergonic and endergonic oxidation-reduction reactions. *Chem Commun* **54** 4091-4099
12. Peters, J. W., Beratan, D. N., Bothner, B., Dyer, R. B., Harwood, C. S., Heiden, Z. M., Hille, R., Jones, A. K., King, P. W., Lu, Y., Lubner, C. E., Minteer, S. D., Mulder, D. W., Raugei, S., Schut, G. J., Seefeldt, L. C., Tokmina-Lukaszewska, M., Zadvornyy, O. A., Zhang, P., and Adams, M. W. (2018) A new era for electron bifurcation. *Curr Opin Chem Biol* **47** 32-38
13. Garcia Costas, A. M., Poudel, S., Miller, A. F., Schut, G. J., Ledbetter, R. N., Fixen, K. R., Seefeldt, L. C., Adams, M. W. W., Harwood, C. S., Boyd, E. S., and Peters, J. W. (2017) Defining electron bifurcation in the electron-transferring flavoprotein family.   *Bacteriol* **199** e00440-00417
14. Toogood, H. S., Leys, D., and Scrutton, N. S. (2007) Dynamics driving function : new insights from electron transferring flavoproteins and partner complexes. *FEBS J.* **274** 5481-5504
15. Tsai, M. H., and Saier, M. H., Jr. (1995) Phylogenetic characterization of the ubiquitous electron transfer flavoprotein families ETF-alpha and ETF-beta. *Res Microbiol* **146** 397-404
16. Chowdhury, N. P., Mowafy, A. M., Demmer, J. K., Upadhyay, V., Koelzer, S., Jayamani, E., Kahnt, J., Hornung, M., Demmer, U., Ermler, U., and Buckel, W. (2014) Studies of the mechanism of electron bifurcation catalyzed by electron transferring flavoprotein (Etf) and butyryl-CoA dehydrogenase (Bcd) of *Acidaminococcus fermentans*   *J. Biol. Chem.* **289** 5145-5157
17. Sato, K., Nishima, Y., and Shiga, K. (2003) Purification of electron-transferring flavoprotein from *Megasphaera elsdenii* and binding of additional FAD with an unusual absorption spectrum. *J. Biochem.* **134** 719-729
18. Weghoff, M. C., Bertsch, J., and Muller, V. (2015) A novel mode of lactate metabolism in strictly anaerobic bacteria. *Environ Microbiol* **17** 670-677

19. Bertsch, J., Parthasarathy, A., Buckel, W., and Muller, V. (2013) An electron-bifurcating caffeyl-Co reductase. *Biol Chem* **288** 11304-11311

20. Brockman, H. L., and Wood, W. A. (1975) D-Lactate dehydrogenase of *Peptostreptococcus elsdenii Bacteriol* **124** 1454-1461

21. Sato, K., Nishina, Y., and Shiga, K. (2013) Interaction between NADH and electron-transferring flavoprotein from *Megasphaera elsdenii J. Biochem.* **153** 565-572

22. Chowdhury, N. P., Kahnt, J., and Buckel, W. (2015) Reduction of ferredoxin or oxygen by flavin-based electron bifurcation in *Megasphaera elsdenii FEBS J.* **282** 3149-3160

23. Edgren, T., and Nordlund, S. (2004) The fixABCX genes in *Rhodospirillum rubrum* encode a putative membrane complex participating in electron transfer to nitrogenase. *Bacteriol* **186**, 2052-2060

24. Ledbetter, R. N., Garcia Costas, A. M., Lubner, C. E., Mulder, D. E., Tokmina-Lukaszewska, M., Artz, J. H., Patterson, A., Magnuson, T. S., Jay, Z. J., Duan, H. D., Miller, J., Plunkett, M. H., Hoben, J. P., Barney, B. M., Carlson, R. P., Miller, A.-F., Bothner, B., King, P. W., Peters, J. W., and Seefeldt, L. C. (2017) The electron bifurcating FixABCX protein complex from *Azotobacter vinelandii* Generation of low-potential reducing equivalents for nitrogenase catalysis. *Biochemistry* **56** 4177-4190

25. Volkl, P., Huber, R., Drobner, E., Rachel, R., Burggraf, S., Trincone, A., and Stetter, K. O. (1993) *Pyrobaculum aerophilum* sp. nov., a novel nitrate-reducing hyperthermophilic archaeum. *Appl Environ Microbiol* **59** 2918-2926

26. Fitz-Gibbon, S. T., Ladner, H., Kim, U. J., Stetter, K. O., Simon, M. I., and Miller, J. H. (2002) Genome sequence of the hyperthermophilic crenarchaeon *Pyrobaculum aerophilum Proc Natl Acad Sci U S A* **99** 984-989

27. Duan, H. D., Lubner, C. E., Tokmina-Lukaszewska, M., Gauss, G. H., Bothner, B., King, P. W., Peters, J. W., and Miller, A. F. (2018) Distinct properties underlie flavin-based electron bifurcation in a novel electron transfer flavoprotein FixAB from *Rhodopseudomonas palustris J Biol Chem* **293** 4688-4701

28. Watmough, N. J., and Frerman, F. E. (2010) The electron transfer flavoprotein: Ubiquinone oxidoreductases. *Biochim. Biophys. Acta* **1797** 1910-1916

29. Demmer, J. K., Bertsch, J., Oppinger, C., Wohlers, H., Kayastha, K., Demmer, U., Ermler, U., and Muller, V. (2018) Molecular basis of the flavin-based electron-bifurcating caffeyl-CoA reductase reaction. *FEBS Lett* **592** 332-342

30. Demmer, J. K., Pal Chowdhury, N., Selmer, T., Ermler, U., and Buckel, W. (2017) The semiquinone swing in the bifurcating electron transferring flavoprotein/butyryl-CoA dehydrogenase complex from *Clostridium difficile Nat Commun* **8** 1577

31. Lubner, C. E., Jennings, D. P., Mulder, D. W., Schut, G. J., Zadvornyy, O. A., Hoben, J. P., Tokmina-Lukaszewska, M., Berry, L., Nguyen, D. M., Lipscomb, G. L., Bothner, B., Jones, A. K., Miller, A. F., King, P. W., Adams, M. W. W., and Peters, J. W. (2017) Mechanistic insights into energy conservation by flavin-based electron bifurcation. *Nat Chem Biol* **13** 655-659

32. Kelley, L. A., Mezulis, S., Yates, C. M., Wass, M. N., and Sternberg, M. J. (2015) The Phyre2 web portal for protein modeling, prediction and analysis. *Nat Protoc* **10** 845-858

33. Song, Y., Nelp, M. T., Bandarian, V., and Wysocki, V. H. (2015) Refining the structural model of a heterohexameric protein complex: surface induced dissociation and o mobility provide key connectivity and topology information. *ACS Cent Sci* **1** 477-487

34. Baud, A., Gonnet, F., Salard, I., Le Mignon, M., Giuliani, A., Mercere, P., Sclavi, B., and Daniel, R. (2016) Probing the solution structure of Factor H using hydroxyl radical protein footprinting and cross-linking. *Biochem J* **473** 1805-1819

35.   Fernandez-Martinez, J., Kim, S. J., Shi, Y., Upla, P., Pellarin, R., Gagnon, M., Chemmama, I. E., Wang, J., Nudelman, I., Zhang, W., Williams, R., Rice, W. J., Stokes, D. L., Zenklusen, D., Chait, B. T., Sali, A., and Rout, M. P. (2016) Structure and function of the nuclear pore complex cytoplasmic mRNA export platform. *Cell* **167** 1215-1228 e1225

36.   Liu, W. H., Roemer, S. C., Zhou, Y., Shen, Z. J., Dennehey, B. K., Balsbaugh, J. L., Liddle, J. C., Nemkov, T., Ahn, N. G., Hansen, K. C., Tyler, J. K., and Churchill, M. E. (2016) The Cac1 subunit of histone chaperone CAF-1 organizes CAF-1-H3/H4 architecture and tetramerizes histones. *Elife* **5**

37.   Mummadisetti, M. P., Frankel, L. K., Bellamy, H. D., Sallans, L., Goettert, J. S., Brylinski, M., Limbach, P. A., and Bricker, T. M. (2014) Use of protein cross-linking and radiolytic footprinting to elucidate PsbP and PsbQ interactions within higher plant Photosystem II. *Proc Natl Acad Sci USA* **111** 16178-16183

38.   Schmidt, C., Zhou, M., Marriott, H., Morgner, N., Politis, A., and Robinson, C. V. (2013) Comparative cross-linking and mass spectrometry of an intact F-type ATPase suggest a role for phosphorylation. *Nat Commun* **4** 1985

39.   Zanphorlin, L. M., Lima, T. B., Wong, M. J., Balbuena, T. S., Minetti, C. A., Remeta, D. P., Young, J. C., Barbosa, L. R., Gozzo, F. C., and Ramos, C. H. (2016) Heat shock protein 90 kDa (Hsp90) has a second functional interaction site with the mitochondrial import receptor Tom70. *Biol Chem* **291** 18620-18631

40.   Merkley, E. D., Rysavy, S., Kahraman, A., Hafen, R. P., Daggett, V., and Adkins, J. N. (2014) Distance restraints from crosslinking mass spectrometry: mining a molecular dynamics simulation database to evaluate lysine-lysine distances. *Protein Sci* **23** 747-759

41.   Hagedoorn, P. L., Chen, T., Schroder, I., Piersma, S. R., de Vries, S., and Hagen, W. R. (2005) Purification and characterization of the tungsten enzyme aldehyde:ferredoxin oxidoreductase from the hyperthermophilic denitrifier *Pyrobaculum aerophilum* *Biol Inorg Chem* **10** 259-269

42.   Elling, F. J., Becker, K. W., Konneke, M., Schroder, J. M., Kellermann, M. Y., Thomm, M., and Hinrichs, K. U. (2016) Respiratory quinones in Archaea: phylogenetic distribution and application as biomarkers in the marine environment. *Environ Microbiol* **18** 692-707

43.   Nguyen, D. M. N., Schut, G. J., Zadvornyy, O. A., Tokmina-Lukaszewska, M., Poudel, S., Lipscomb, G. L., Adams, L. A., Dinsmore, J. T., Nixon, W. J., Boyd, E. S., Bothner, B., Peters, J. W., and Adams, M. W. W. (2017) Two functionally distinct NADP$^+$-dependent ferredoxin oxidoreductases maintain the primary redox balance of *Pyrococcus furiosus* *Biol Chem* **292** 14603-14616

44.   Iyanagi, T. (1977) Redox properties of microsomal reduced nicotinamide adenine dinucleotide-cytochrome b_5 reductase and cytochrome b_5 *Biochemistry* **16** 2725-2730

45.   Medina, M., Gomez-Moreno, C., and Cammack, R. (1995) Electron spin resonance and electron nuclear double resonance studies of flavoproteins involved in the photosynthetic electron transport in the cyanobacterium *Anabaena sp.* PCC 7119. *Eur J Biochem* **227** 529-536

46.   DeRose, V. J., Woo, J. C., Hawe, W. P., Hoffman, B. M., Silverman, R. B., and Yelekci, K. (1996) Observation of a flavin semiquinone in the resting state of monoamine oxidase B by electron paramagnetic resonance and electron nuclear double resonance spectroscopy. *Biochemistry* **35**, 11085-11091

47.   Deistung, J., and Thorneley, R. N. F. (1986) Electron transfer to nitrogenase. Characterization of flavodoxin from *Azotobacter chroococcum* and comparison of its redox potentials with those of flavodoxins from *Azotobacter vinelandii* and *Klebsiella pneumoniae* (nifF-gene product). *Biochem. J.* **239** 69-75

48.   Bergdoll, L., Ten Brink, F., Nitschke, W., Picot, D., and Baymann, F. (2016) From low- to high-potential bioenergetic chains: Thermodynamic constraints of Q-cycle function. *Biochim Biophys Acta* **1857** 1569-1579

49.   Page, C. C., Moser, C. C., Chen, X., and Dutton, P. L. (1999) Natural engineering principles of electron tunnelling in biological oxidation-reduction. *Nature* **402** 47-52

50.   Peregrina, J. R., Sanchez-Azqueta, A., Herguedas, B., Martinez-Julvez, M., and Medina, M. (2010) Role of specific residues in coenzyme binding, charge-transfer complex formation, and catalysis in *Anabaena* ferredoxin NADP$^+$-reductase. *Biochim Biophys Acta* **1797** 1638-1646

51.   Batie, C. J., and Kamin, H. (1986) Association of ferredoxin-NADP$^+$ reductase with NADP(H) specificity and oxidation-reduction properties. *Biol Chem* **261** 11214-11223

52.   Zhang, P., Yuly, J. L., Lubner, C. E., Mulder, D. W., King, P. W., Peters, J. W., and Beratan, D. N. (2017) Electron bifurcation: thermodynamics and kinetics of two-electron brokering in biological redox chemistry. *Acc Chem Res* **50** 2410-2417

53.   Nitschke, W., and Russell, M. J. (2012) Redox bifurcations: mechanisms and importance to life now, and at its origin: a widespread means of energy conversion in biology unfolds. *Bioessays* **34** 106-109

54.   Lin, T. Y., Werther, T., Jeoung, J. H., and Dobbek, H. (2012) Suppression of electron transfer to dioxygen by charge transfer and electron transfer complexes in the FAD-dependent reductase component of toluene dioxygenase. *Biol Chem* **287** 38338-38346

55.   Sena, F. V., Sousa, F. M., Oliveira, A. S. F., Soares, C. M., Catarino, T., and Pereira, M. M. (2018) Regulation of the mechanism of Type-II NADH: Quinone oxidoreductase from *S. aureus Redox Biol* **16** 209-214

56.   Berry, L., Poudel, S., Tokmina-Lukaszewska, M., Colman, D. R., Nguyen, D. M. N., Schut, G. J., Adams, M. W. W., Peters, J. W., Boyd, E. S., and Bothner, B. (2018) H/D exchange mass spectrometry and statistical coupling analysis reveal a role for allostery in a ferredoxin-dependent bifurcating transhydrogenase catalytic cycle. *Biochim Biophys Acta* **1862** 9-17

57.   Lipscomb, G. L., Stirrett, K., Schut, G. J., Yang, F., Jenney, F. E., Jr., Scott, R. A., Adams, M. W., and Westpheling, J. (2011) Natural competence in the hyperthermophilic archaeon *Pyrococcus furiosus* facilitates genetic manipulation: construction of markerless deletions of genes encoding the two cytoplasmic hydrogenases. *Appl Environ Microbiol* **77** 2232-2238

58.   Verhagen, M. F., Menon, A. L., Schut, G. J., and Adams, M. W. (2001) *Pyrococcus furiosus large-scale cultivation and enzyme purification. *Methods Enzymol* **330** 25-30

59.   Zehnder, A. J., and Wuhrmann, K. (1976) Titanium (III) citrate as   nontoxic oxidation-reduction buffering system for the culture of obligate anaerobes. *Science* **194** 1165-1166

60.   Efimov, I., Parkin, G., Millett, E. S., Glenday, J., Chan, C. K., Weedon, H., Randhawa, H., Basran, J., and Raven, E. L. (2014) A simple method for the determination of reduction potentials in heme proteins. *FEBS Lett* **588** 701-704

61.   Massey, V. (1991) A simple method for determination of redox potentials. in *Flavins and flavoproteins.* (Curti, B., Ronchi, S., and Zanetti, G. eds.), Walter de Gruyer, Berlin. pp 59-66

62.   Trimmer, E. E., Ballou, D. P., Galloway, L. J., Scannell, S. A., Brinker, D. R., and Casas, K. R. (2005) Aspartate 120 of *Escherichia coli* methylenetetrahydrofolate reductase: evidence for major roles in folate binding and catalysis and a minor role in flavin reactivity. *Biochemistry* **44** 6809-6822

63.   Yang, Z. Y., Ledbetter, R., Shaw, S., Pence, N., Tokmina-Lukaszewska, M., Eilers, B., Guo, Q., Pokhrel, N., Cash, V. L., Dean, D. R., Antony, E., Bothner, B., Peters, J. W., and Seefeldt, L. C. (2016) Evidence that the Pi release event is the rate-limiting step in the nitrogenase catalytic cycle. *Biochemistry* **55** 3625-3635

64.   Poudel, S., Tokmina-Lukaszewska, M., Colman, D. R., Refai, M., Schut, G. J., King, P. W., Maness, P. C., Adams, M. W., Peters, J. W., Bothner, B., and Boyd, E. S. (2016) Unification of [FeFe]-hydrogenases into three structural and functional groups. *Biochim Biophys Acta* **1860** 1910-1921

65.   Zhang, H., Wen, J., Huang, R. Y., Blankenship, R. E., and Gross, M. L. (2012) Mass spectrometry-based carboxyl footprinting of proteins: method evaluation. *Int J Mass Spectrom* **312** 78-86

66.   Luo, M. L., Jackson, R. N., Denny, S. R., Tokmina-Lukaszewska, M., Maksimchuk, K. R., Lin, W., Bothner, B., Wiedenheft, B., and Beisel, C. L. (2016) The CRISPR RNA-guided surveillance complex in *Escherichia coli* accommodates extended RNA spacers. *Nucleic Acids Res* **44** 7385-7394

67.   Biasini, M., Bienert, S., Waterhouse, A., Arnold, K., Studer, G., Schmidt, T., Kiefer, F., Gallo Cassarino, T., Bertoni, M., Bordoli, L., and Schwede, T. (2014) SWISS-MODEL: modelling protein tertiary and quaternary structure using evolutionary information. *Nucleic Acids Res* **42** W252-258

68.   Pettersen, E. F., Goddard, T. D., Huang, C. C., Couch, G. S., Greenblatt, D. M., Meng, E. C., and Ferrin, T. E. (2004) UCSF Chimera--a visualization system for exploratory research and analysis. *J Comput Chem* **25** 1605-1612
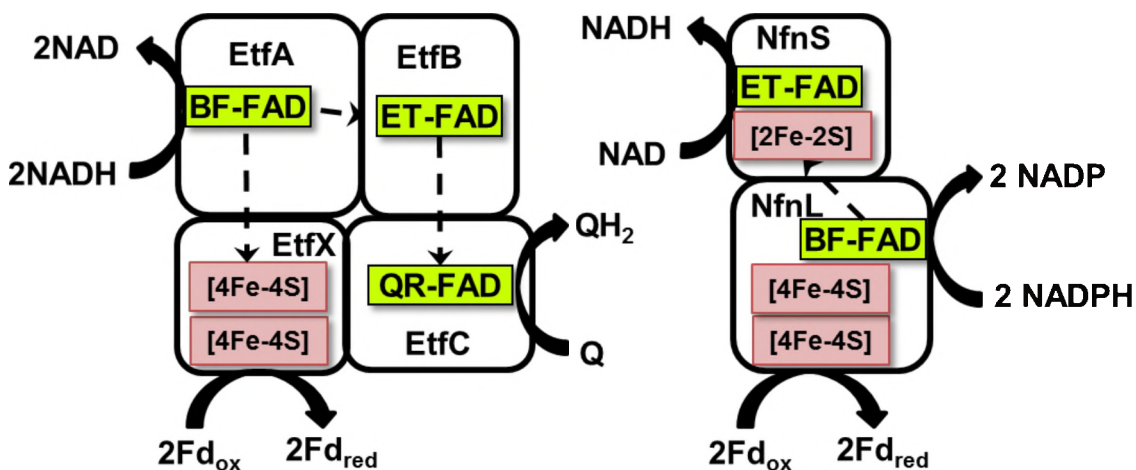
Figure 1. Cofactor content and proposed pathway of electron flow in *P. aerophilum* EtfABCX and *P. furiosus* NfnI. The abbreviations are: BF-FAD, bifurcating flavin; ET-FAD, electron transfer flavin; QR-FAD, quinone reductase flavin; Q, quinone; QH_2, reduced quinone; Fd_{ox}, oxidized ferredoxin; Fd_{red}, reduced ferredoxin.
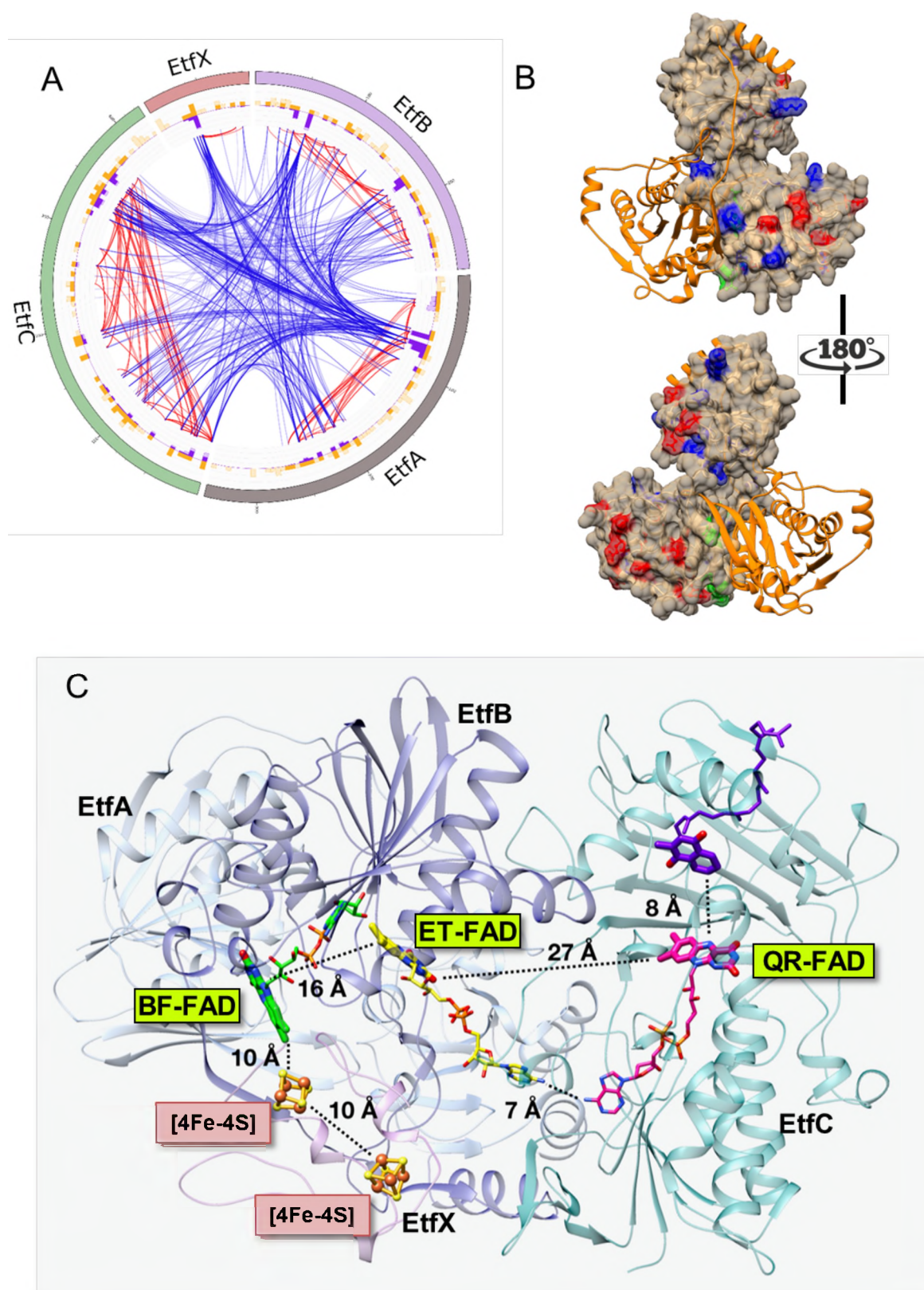
Figure 2. A). The multi-layer circular plot presents interactions within the Pae EtfABCX complex captured by cross-linking (BS3). The most outer layer represents the protein sequence: EtfA is in gray, EtfB is in purple, EtfC is in green and EtfX is in pink. Yellow and purple histograms show the location of BS3 target residues (Lys, Ser) and the density of cross-links, respectively. Blue lines represent connections between subunits (inter-subunit cross-links) and red lines highlight interactions within a single unit (intra-subunit cross-links). Cross-links maintaining less than 20 ppm error and a score higher than 3 (score >2 is considered significant) are displayed. **B).** Protein surface map of the complete Pae EtfABCX complex (for simplicity only the AB dimer is presented) shows GEE (modification sites shown in red) and DnsCl (modification sites shown in blue) labels incorporated in to the native complex during short exposure to the two labeling reagents. Residues at the dimer interface highlighted in green correspond to labels integrated into the structure exclusively in the latest time points. Individual proteins are color coded as follows: EtfB in orange; EtfA in tan. **C).** Ribbon diagram of the MS-validated EtfABCX model. EtfA and EtfB are in light and dark blue, respectively, EtfC is in teal and EtfX is in magenta, the BF-FAD is in green, the ET-FAD in yellow and the QR-FAD in pink. Organic cofactors are shown using thick sticks to emphasize the redox-active portions and thin sticks to complete the structures. Iron-sulfur clusters are in orange (Fe) and yellow (S) and the menaquinone (purple) was modeled using the 2GMH (Porcine electron transfer flavoprotein-ubiquinone oxidoreductase) structure with bound ubiquinone.
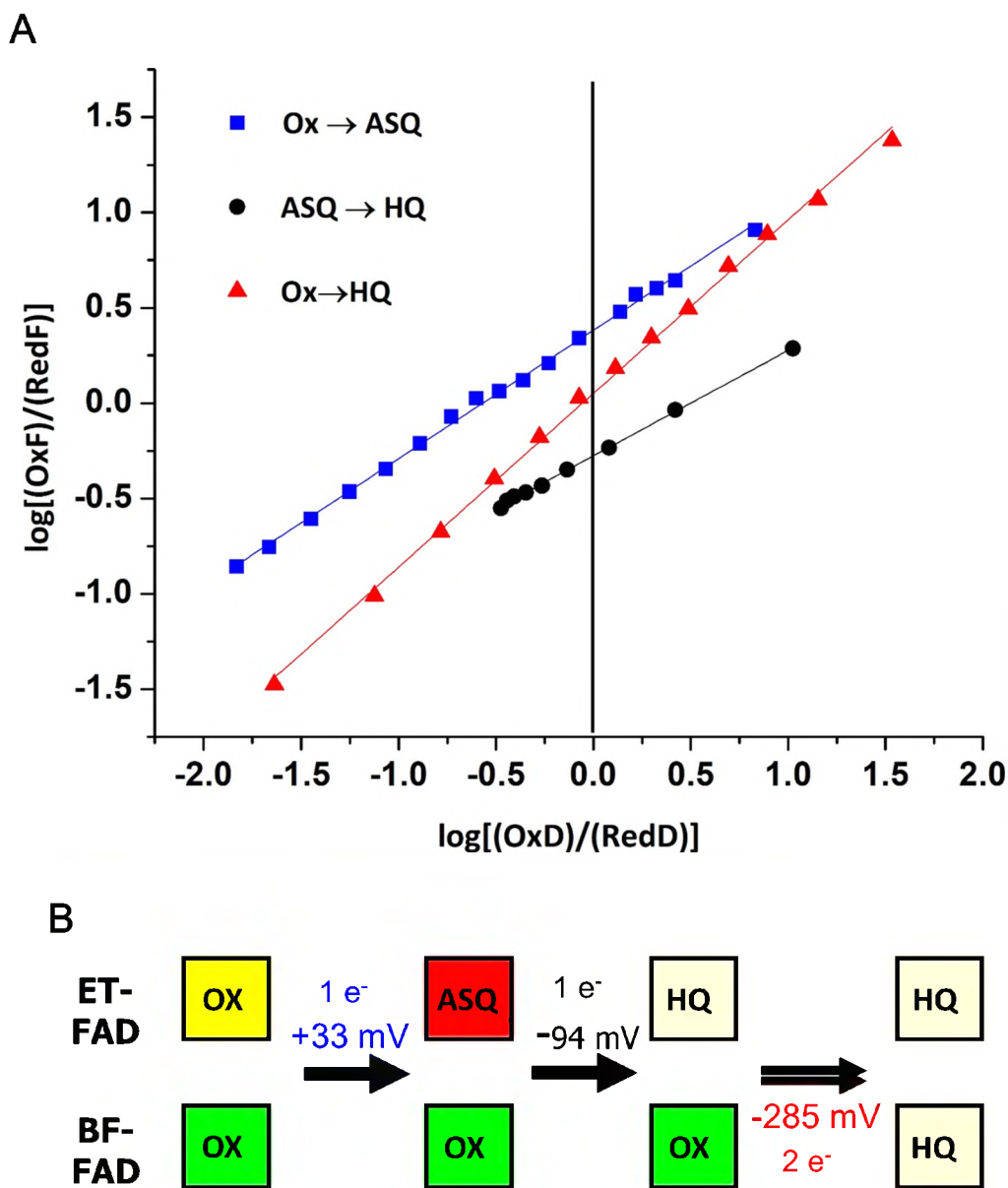
Figure 3. A Slopes of Nernst plots confirm the 1 e^- nature of events in phases 1 and 2, and the 2 e^- nature of phase 3. Best linear fits are: phase 1 (blue): 0.66x + 0.55 (R^2 = .997), phase 2 (black):0.55x - 0.27 (R^2 = .999), and phase 3 (red) 0.91 x + 0.05 (R^2 = .998). For the data in blue the 'oxidized' flavin is OX, 'reduced' flavin is the ASQ and the dye is thionine. For the data in black the 'oxidized' flavin is ASQ, 'reduced' flavin is the HQ and the dye is nile blue. For the data in red 'oxidized' flavin is OX, 'reduced' flavin is HQ and the dye is safranin-O. **B.** Proposed reduction events for each FAD cofactor in EtfAB and the measured potentials.
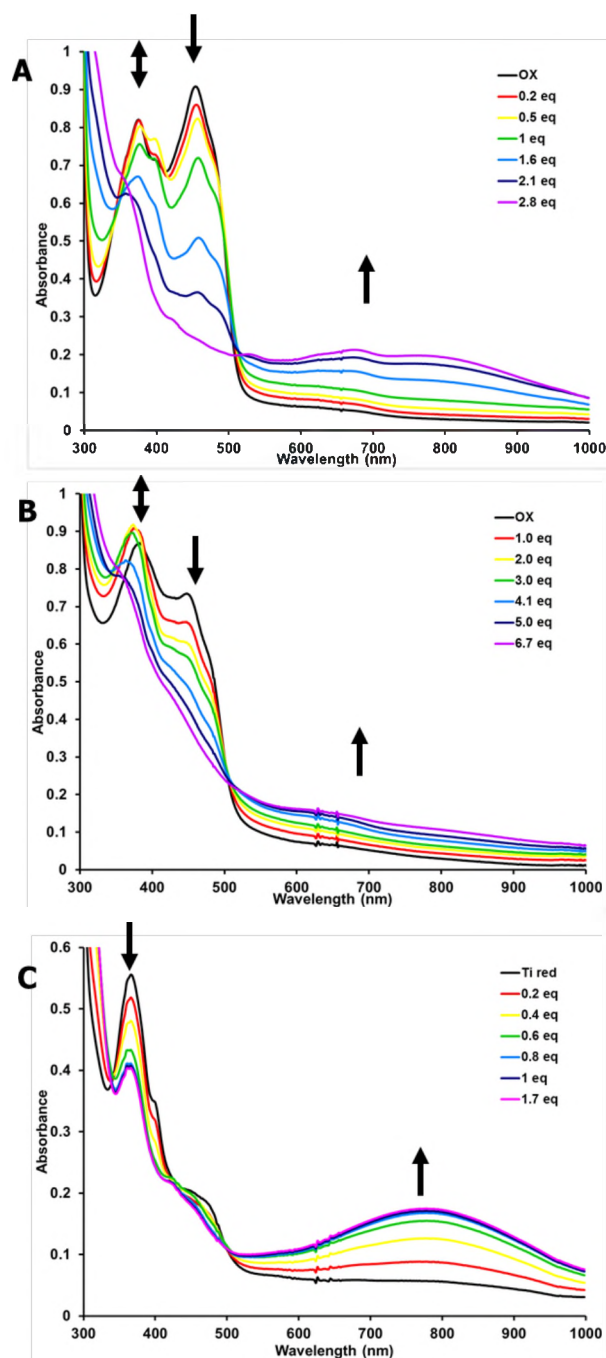
22

Figure 4. Titration of **A)** *Pae* EtfAB (74 μM) and **B)** EtfABCX (15 μM) with NADH. Arrows (left to right) indicate formation and disappearance of the ASQ, disappearance of OX flavin absorbance and the formation of a broad CT complex. **C)**. Anaerobic titration with NAD^+ of *Pae* EtfAB (74 μM) reduced with excess Ti-citrate. Arrows (left to right) indicate disappearance of ASQ and the formation of a broad CT complex.
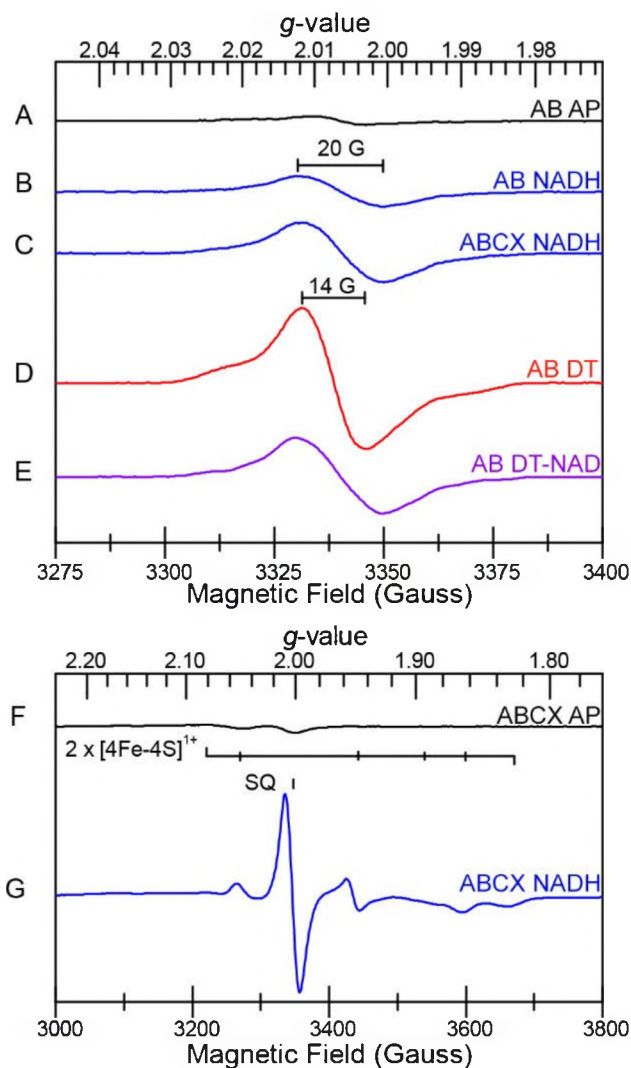
Figure 5. EPR spectra (9.38 GHz CW) of *Pae* EtfAB and EtfABCX. The samples are: **AB AP**, As-purified EtfAB; **AB NADH**, EtfAB treated with NADH; **ABCX NADH**, EtfABCX treated with NADH; **AB DT**, EtfAB treated with Na-dithionite; **AB DT-NAD**, EtfAB sequentially treated with Na-dithionite and NAD$^+$; **ABCX AP,** EtfABCX as purified; **ABCX NADH**, EtfABCX treated with NADH. Top spectra (A-E) were recorded at 77 K and bottom spectra (F, G) were recorded at 10 K.
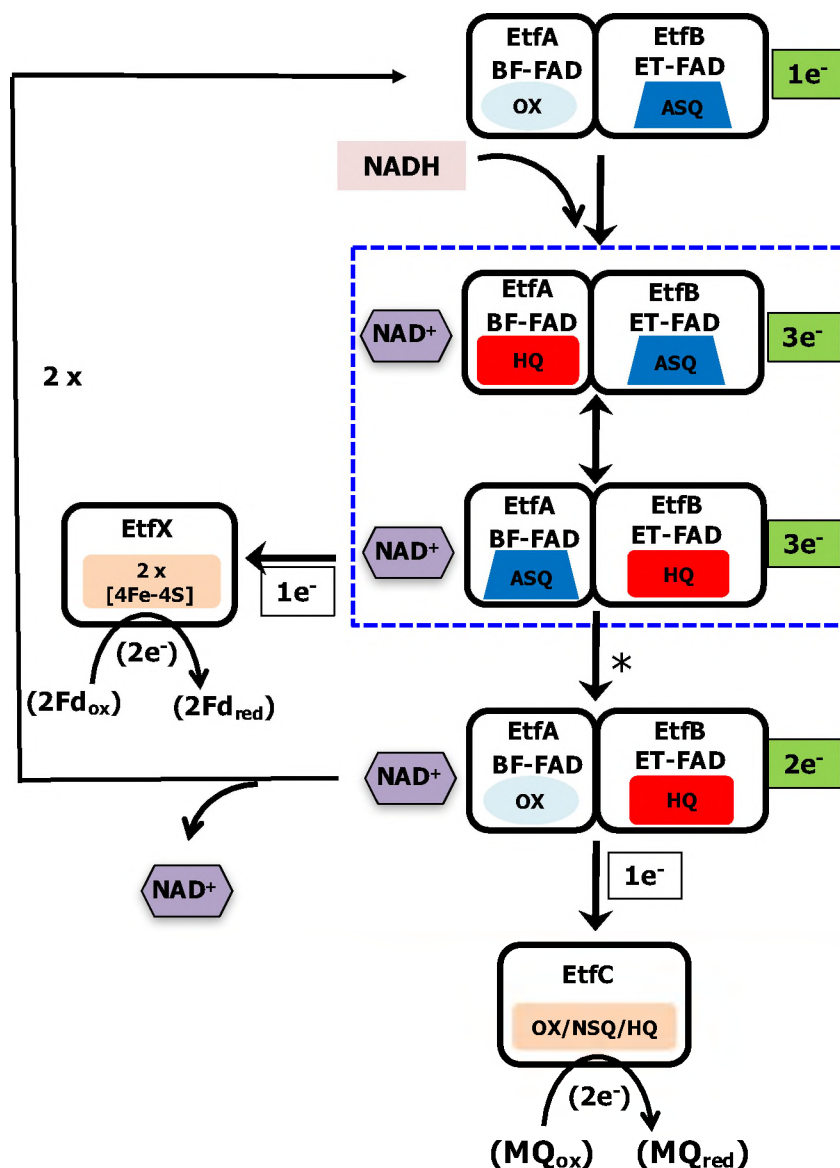
Figure 6. Proposed catalytic cycle of EtfABCX. The complex is depicted in its bifurcation ready state in which the ET-FAD is in the ASQ state. In the first round of NADH oxidation, the BF-FAD is reduced to the HQ state and forms a CT complex with NAD$^+$. The first electron is transferred to the ASQ-ET-FAD to generate the HQ state, leaving the ASQ-BF-FAD. The transfer of an electron to the low potential branch [4Fe-4S] cluster triggers a protein conformational change (indicated by the asterisk) that then enables HQ-ET-FAD to reduce the FAD of EtfC with 1 e$^-$ converting it to the NSQ state. The catalytic cycle continues with the oxidation of a second NADH and the transfer of electrons down the low and high potential branches leading to the reduction of ferredoxin (Fd) and menaquinone (MQ), respectively. Boxed with a blue dotted line are the complexes with NAD$^+$ that could form CT complexes.

The catalytic mechanism of electron bifurcating electron transfer flavoproteins (ETFs) involves an intermediary complex with NAD $^+$

Gerrit J. Schut, Nishya Mohamed-Raseek, Monika Tokmina-Lukaszewska, David W. Mulder, Diep M. N. Nguyen, Gina L. Lipscomb, John P. Hoben, Angela Patterson, Carolyn E. Lubner, Paul W. King, John W. Peters, Brian Bothner, Anne-Frances Miller and Michael W. W. Adams

J. Biol. Chem. published online December 19, 2018

Alerts:
- When this article is cited
- When a correction for this article is posted

Click here to choose from all of JBC's e-mail alerts